



The Influence of Boundary Layers on Supersonic Inlet Unstart

H. Do¹ and S. Im²

Mechanical Engineering Department, Stanford University, Stanford, CA 94305

M. G. Mungal³

Mechanical Engineering Department, Stanford University, Stanford, CA 94305
School of Engineering, Santa Clara University, Santa Clara, CA 95053

and

M. A. Cappelli⁴

Mechanical Engineering Department, Stanford University, Stanford, CA 94305

A transverse air jet injected into a Mach 5 model inlet flow generated by an in-draft supersonic wind tunnel, is used to induce inlet unstart. Planar Laser Rayleigh Scattering (PLRS) from condensed CO₂ particles in the tunnel flow is used to visualize the unsteady flow during unstart. Simultaneously, pressure traces along the wind tunnel are recorded with high speed pressure sensors attached to the bottom wall of the wind tunnel. A series of time synchronized PLRS images reveals that a shock system, followed by flow separation, originating from the jet injection nozzle propagates upstream. The flow then unstarts upon the arrival of the shock at the inlet. Studies conducted using three different inlet model geometries indicate that the presence of turbulent wall boundary layers strongly affect the unstart dynamics. It is found that relatively thick turbulent boundary layers result in faster inlet unstart, when compared to thin, laminar boundary layers.

Nomenclature

| | | |
|----------|---|--|
| γ | = | ratio of specific heats |
| Ma, M | = | Mach number |
| p | = | static pressure |
| p_0 | = | stagnation pressure |
| ρ | = | density |
| R | = | square root of the ratio of the jet momentum flux to that of the free stream |
| T_0 | = | stagnation temperature |

I. Introduction

INLET unstart has been described as the disengagement of a shock system at the inlet of a scramjet/ramjet engine.¹ If not avoided, it can cause in-flight engine malfunctioning.²⁻⁹ Most frequently occurring during the transition to ramjet/scramjet mode in the flight Mach number range of 3 to 6,¹⁰ unstart is believed to be caused by the thermal choking¹¹ of the internal supersonic flow triggered by increased heat release in the combustor.¹²⁻¹⁴ The heat release in the combustor is followed by a pressure rise in the inlet/isolator and boundary layer separation/growth, reducing the core flow area, and forcing the internal flow into a subsonic regime.¹⁵ In a ground test facility that mimics the

¹ Postdoctoral Researcher, Mechanical Engineering, Stanford University.

² Graduate Student, Mechanical Engineering, Stanford University, AIAA Student Member.

³ Dean of Engineering, Santa Clara University, Professor Emeritus, Mechanical Engineering, Stanford University, AIAA Associate Fellow.

⁴ Professor, Mechanical Engineering, Stanford University.

thermal choking by the movement of a mechanical flap placed downstream, Wagner et al.^{8,9,16} confirmed the presence of the separated boundary layer using Particle Image Velocimetry (PIV), and captured (via high speed Schlieren photography) the formation and dynamics of an unstart shock system that interacted with the boundary layers.

Past studies have examined the use of boundary layer bleeding,¹⁴ isolators^{13,17-19} and vortex generator jets,²⁰ as various means of avoiding or delaying inlet unstart. All of these methods seek to influence the evolution of the boundary layer during the upstream propagation of flow disturbances that originate from the combustor. Recording and understanding the dynamics of boundary layer evolution during unstart is critical to the development of such unstart mitigation strategies. Studies will therefore require diagnostic methods that are capable of resolving the structure of boundary layers, and shock-boundary layer interactions.

This paper describes a study of the unstart in a supersonic model inlet, triggered by mass injection downstream of the inlet. The jet/supersonic flow and ensuing dynamics are highly three-dimensional, and we visualize the unstart flow features (e.g. boundary layers, shock-boundary layer interactions) using Planar Laser Rayleigh Scattering (PLRS) from condensed CO₂ particles (particulate fog). Miles and Lempert,²¹ Wu et al.,²² and Poggie et al.²³ have demonstrated the general utility of this diagnostic for low temperature/pressure supersonic flows expanded through the diverging nozzle of a supersonic wind tunnel of low (ambient) stagnation temperature. Weak (e.g., oblique) shocks are visualized as demarcations in intensity as a result of the post-shock increase in density (and hence particles). However, regions of elevated temperature can cause particle sublimation, and therefore boundary layers and regions behind strong (normal) shocks lack particles and appear dark, with very strong contrasts. While qualitative at this time, this diagnostic captures flow features with high spatial discrimination (unlike Schlieren photography, which is line-of-sight), and reveals flow dynamics suitable for quantitative characterization, e.g., of regions of boundary layer transition, slip lines, and the propagation of both weak and strong shockwaves.

The use of this PLRS visualization allows us to investigate the evolution of fine scale flow structures under unstart flow conditions produced in a model inlet built into a supersonic wind tunnel.²⁴ The current study reveals that the flow features emerging during unstart are influenced by wall boundary layer conditions, which, in some cases, can either delay or accelerate the inlet unstart process.

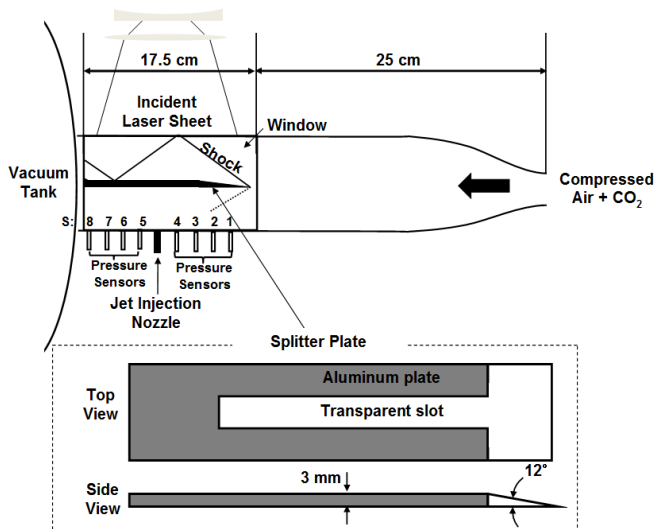


Figure 1. Experimental setup including a Mach 5 wind tunnel, pressure sensors and PLRS imaging system.

mostly generated at various junctions in the gas stream inlet piping. The static pressure and temperature of the flow in the test section is approximately 1 kPa and 50 K, respectively.

II. Experimental Setup

The experimental facility consists of a $Ma = 5$ wind tunnel, an integrated laser system and a jet injection module.

A schematic of the $Ma = 5$ wind tunnel is shown in Fig. 1. High pressure air ($p_0 = 350$ kPa and $T_0 = 300$ K) containing CO₂ (approximately 25 % by volume) expands through a converging/diverging nozzle (25:1 area ratio) to establish a relatively uniform $Ma = 5$ flow in a rectangular test section (4 cm \times 4 cm cross-sectional area). The exit of the tunnel is connected to a vacuum tank that accommodates the incoming mass flow for approximately 5 seconds of run time. During this run time, the vacuum tank pressure is maintained at values lower than the static pressure in the test section. A honeycomb panel 2.5 cm in length comprising 3 mm hexagonal cells is placed upstream of the converging nozzle to suppress flow swirling,

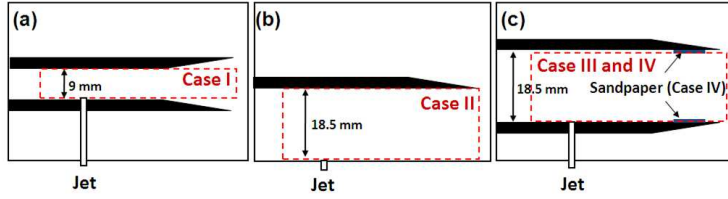


Figure 2. The region of interest in each case (Case I through Case IV) and configurations of the splitter plates.

flow in the lower half (Case II in Fig. 2 (b)). In this configuration (Case II), the jet (ID = 3 mm) is injected through a relatively thick boundary layer (which originated upstream near the throat of the tunnel) into the flow of the model inlet/isolator defined in the lower half of the tunnel. The boundary layer on the upper wall of this inlet (i.e. on the bottom surface of the splitter plate) grows naturally from the leading edge of the plate. Three other model inlet/isolator configurations are studied. All of the configurations are summarized in Fig. 2, which also depicts the flow regions imaged by planar Rayleigh scattering (indicated qualitatively by the rectangles defined by the dashed lines).

Static pressure traces on the bottom wall of the tunnel are recorded using eight fast response (100 kHz) pressure sensors (S1 – S8: PCB Piezotronics, Model 113A26). This provides measurements of the temporal evolution in pressure on the lower wall of the Case II model inlet/isolator flow configurations. At this time, this is the only configuration for which we have pressure data. The sensors and the jet injection nozzle, placed between S4 and S5, (see Fig. 1) are separated by 15 mm along the centerline of the bottom wall parallel to the freestream flow direction: S1 and S8 are located 60 mm upstream and downstream from the nozzle, respectively. The distance between the tip of the splitter plate (270 mm downstream from the converging/diverging nozzle throat) and the jet nozzle is 75 mm.

The experimental components for Rayleigh scattering include a Nd:YAG laser (New Wave, Gemini PIV) capable of generating approximately 100 mJ/pulse (532 nm wavelength) energy with 10 Hz pulse repetition, an unintensified CCD camera (La Vision, Imager Intense) and a computer (not shown) to facilitate data acquisition. The laser beam is formed into a thin sheet of 0.5 mm thickness to illuminate the test section using a combination of two concave cylindrical lenses and a convex spherical lens. Scattered light is captured by the camera along a direction normal to the laser sheet. Laser firing is synchronized with the CCD camera exposure (3 μ s shutter). One of the laser pulses is selected to trigger the jet injection module while the tunnel is operating, but delayed as desired by a pulse delay generator (SRS, DG 535) to take time resolved images at different phases in the flow evolution induced by the jet injection. The jet injection is controlled by a solenoid valve (ASCO, Red Hat II) driven by a controller (Optimal Engineering System Inc.) receiving the trigger signal from the delay generator. A sonic jet (air, in these studies presented here) is injected into the test section through a 3 mm diameter hole in the bottom wall resulting in a flow disturbance and an overall increase in flow pressure and temperature. Relevant to the jet interaction and mixing with the supersonic free stream is the square root of the ratio of the jet momentum flux to that of the free stream, defined by:

$$R = \sqrt{\frac{(\rho u^2)_{jet}}{(\rho u^2)_{\infty}}} = \sqrt{\frac{(\gamma p M^2)_{jet}}{(\gamma p M^2)_{\infty}}}$$

Here, ρ , u , γ , p , and M are air density, velocity, ratio of specific heats, pressure and Mach number of the jet (subscript *jet*) and freestream (subscript ∞) flow, respectively.

III. Results

A. Unstart: Planar Laser Rayleigh Scattering (PLRS)

The inlet geometry of Case I (Fig. 2 (a)) is used to simulate inlet/isolator flows in the presence of multiple shock/expansion reflections that compress and decelerate the incoming flows. Here, two identical splitter plates isolate the flow in the model inlet defined between the plates separated by 9 mm. A downstream air jet ($R = 3.5$) is injected into the inlet to induce unstart.

A set of time synchronized planar laser Rayleigh scattering (PLRS) images (Fig. 3) illustrates the evolution of the flow structure while the flow unstarts. The flow structure, including shock/expansion reflections through the

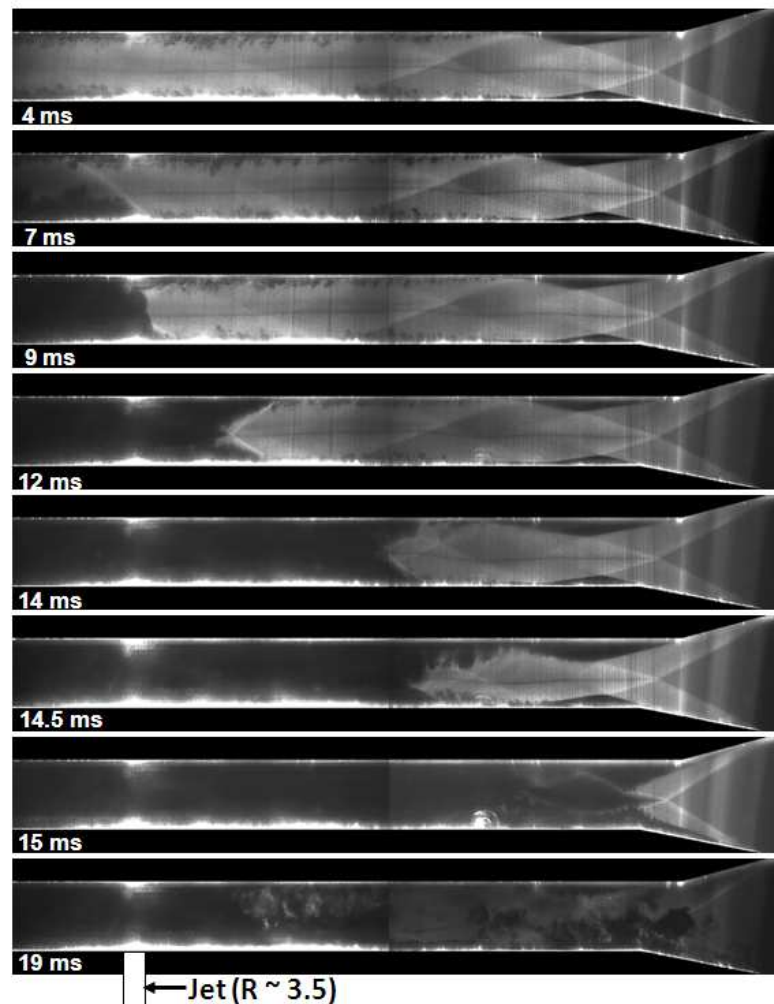


Figure 3. Time sequential PLRS images revealing flow evolution with Case I model inlet geometry.

flow channel (Case I) before the jet is injected into the flow is visualized in the 4 ms panel of Fig. 3. At this time, 4 ms after the trigger signal activating the solenoid valve, the jet fluid has not yet arrived at the nozzle exit. At 7 ms, a jet inducing a bow shock appears and then appears to propagate upstream of the jet nozzle by 9 ms, and is followed by flow separation of both the top and bottom boundary layers (9 – 14.5 ms). These flow disturbances (e.g. shockwave, boundary layer growth/separation) reach the inlet lip, unstarting the flow, by 19 ms. At that moment, the flow near the inlet lip appears to be very unstable and the entire flow channel becomes dark due to the sublimation of the solid CO_2 particles, confirming complete inlet unstart. We see then that the downstream flow appears to unchoke by the excessive mass loading producing flow disturbances that move upstream to unstart the model inlet. We believe that the propagation of these flow disturbances may be facilitated by the presence of thicker boundary layers on the surfaces of the model inlet, and so we tested three other initial boundary layer conditions (Cases II through IV, height of the model inlets is 18.5 mm) with fixed R (4.5) to investigate the influence of the boundary layers on this unstart behavior. For the Case II geometry, our study of this process is further facilitated by pressure taps on the lower surface of the model inlet, which is also the tunnel lower wall, where a relatively thick turbulent boundary layer develops (Sec. B).

B. Unstart: Pressure Measurement

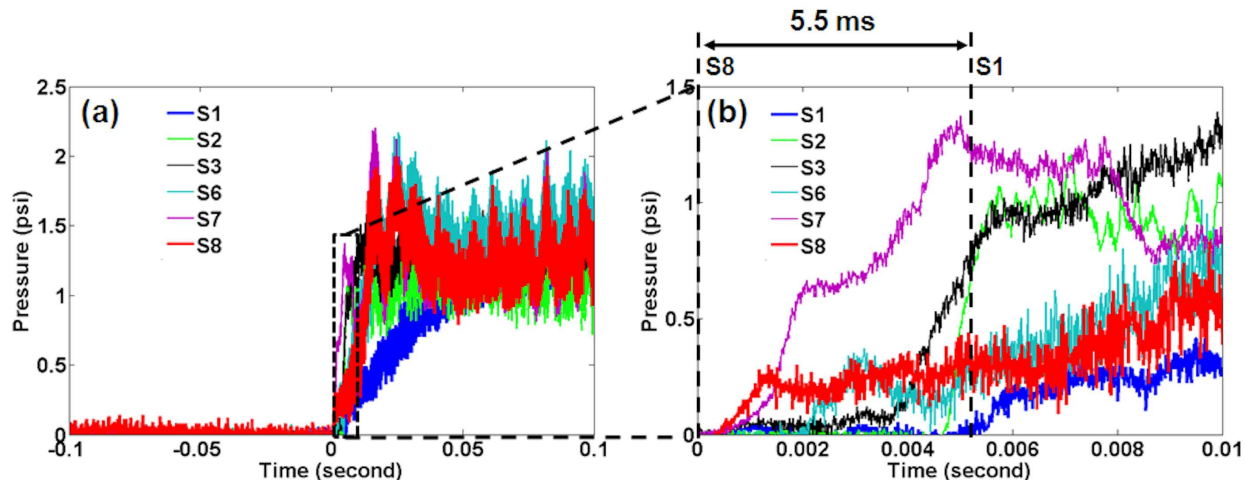


Figure 4. Pressure traces recorded on the bottom wall of the wind tunnel.

The unstart dynamics induced by air jet injection is clearly reflected in the pressure traces measured on the bottom surface of the wind tunnel (Case II). Figure 4 (a) documents the sudden pressure rise at the various locations on the lower wall (recall that the nozzle located between S4 and S5). The time reference ($t = 0$ sec) in this figure corresponds to the moment when the pressure first rises at the sensor located at S8 (i.e., the farthest downstream region characterized). The pressure at S8 starts to rise abruptly at approximately 10 ms after the jet injection trigger signal to open the solenoid valve. Absolute pressure offsets are subtracted from the traces to illustrate relative differences between the pressure recorded before and after the jet injection. The pressure traces recorded at the locations nearest to the jet nozzle (S4 and S5, not shown) fluctuate significantly, due to flow instabilities in the near field of the jet. It is noteworthy that the first pressure increase is recorded at S8 and this high pressure region then

expands towards the upstream region of the tunnel, presumably along the subsonic boundary layer, in succession through to the location at S1 (Fig. 4 (b)). This ordering in the rise in pressure confirms that unchoking originates downstream of the jet injection point, triggering tunnel unstart, i.e., the transition to subsonic flow. We conjecture that the unchoking of the flow, i.e. the subsonic flow caused by mass injection, first appears far downstream near the model exit due to the reduced supersonic core flow area by the growth of boundary layers on the tunnel surfaces and the mass addition. The propagation of this high pressure region from S8 to S1 (over 12 cm distance) takes approximately 5.5 ± 0.5 ms (see Fig. 4 (b)) indicating that this pressure wave propagates at a speed of approximately 22 ± 2 m/s (a mean of 4 measurements). For comparison the freestream speed is approximately 720 m/s.

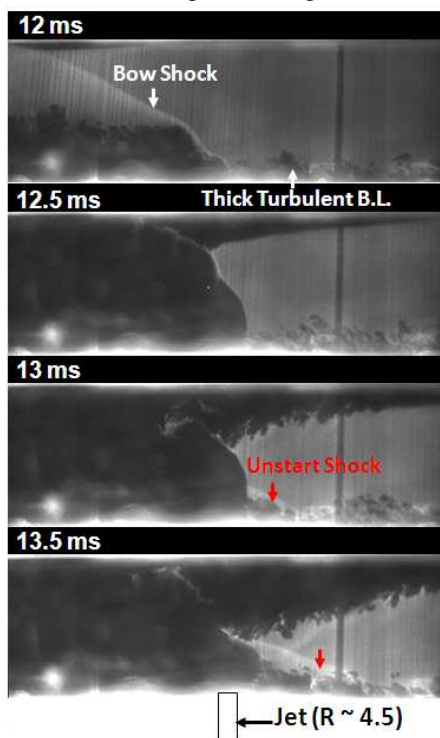


Figure 5. Time sequential PLRS images taken in the region adjacent to the jet for Case II.

C. Asymmetric Wall Boundary Layer Conditions

Here, we discuss the model inlet unstart dynamics, as depicted by the PLRS studies, induced by the injected mass for the Case II model configuration (Fig. 2). This case, for which we describe the pressure traces in Sec. B above, is referred to here as having an *asymmetric* wall boundary condition, in that it is primarily distinguished by the presence of a thick turbulent boundary layer on the inlet wall through which the jet is injected. Under the current flow condition, the model inlet is found to unstart at about 21 ms after the jet is triggered (or 11 ms following the first recording of a pressure disturbance at S8).

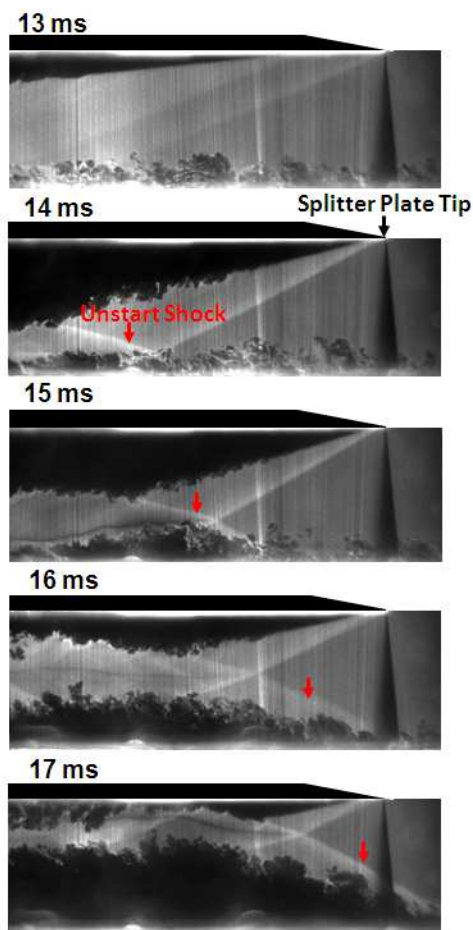


Figure 6. Time sequential PLRS images taken in the first 5 cm region downstream of the splitter for Case II.

thin and initially laminar, while in Case IV both walls have relatively thick turbulent boundary layers prior to jet injection.

We find that with the Case III configuration, the oblique unstart shock that was seen to emerge in Case II *does not appear*, and, as a consequence, unstart is significantly delayed in comparison with other cases. Figure 7 presents the PLRS images for the two frames spanning the entire region of interest, depicting the inlet flow observed for Case III over a time ranging from just prior to jet injection through to unstart. Unstart appears to occur at a time of 55 ms after jet triggering in this case. As shown in Fig. 7 (a), (taken in the absence of the jet), the two splitter plates (with outward facing wedge) isolate the main flow from the turbulent boundary layers on the tunnel walls to define this model inlet configuration. Thin (initially laminar) boundary layers form on both upper and lower walls. Weak shock waves appear originating from the splitter tips, most likely due to the small but finite dimensions of the tips. Note that the interaction of the shock originating from the lower wall induces flow separation on the upper wall, at a downstream location of approximately 40 mm. The flow is seen to undergo a laminar-to-turbulent flow transition, with the clear indication of relatively thin turbulent boundary layers in the downstream frame. Figure 7(b) is a similar depiction, taken after jet injection (approximately 17 ms after jet triggering). At this time, we see from the brighter region that spans across the inlet at approximately 20 mm upstream of the jet, that a compression wave (presumably leading a pseudo-shock region) forms, almost normal to the flow direction, as indicated by the diffuse, brighter signal at the center of the channel. This compression is followed by the apparent thickening of the turbulent boundary layers on both top and bottom surfaces. This compression wave propagates upstream and arrives at a position of about 27 mm from the splitter tip within about 1 ms (see Fig. 7(c)) and remains there (appears quasi-steady) for approximately 37 ms (from 18 ms to 55 ms). This wave is thicker than typical shockwaves such as the oblique unstart shock seen in Case II, or the incident shocks originating from the splitter tips, and is not strong enough to cause transition to subsonic flow. This is evident from the fact that we still see significant Rayleigh

The time sequential images in Figs 5 and 6 illustrate the evolution in the flow while the inlet undergoes unstart by an air jet of $R = 4.5$. The entire flow region of interest (designated by the dashed rectangular region in Fig. 2 (b)) is interrogated in two separate Rayleigh scattering frames. The first frame illuminates the region in the vicinity of the jet nozzle (Fig. 5), and the other, the upstream region near the tip of the splitter plate (Fig. 6). Each imaging region covers a 5 cm width along the flow direction (from right to the left) and an 18.5 mm height. When combined, these two frames span the region within the dashed rectangular lines for Case II, in Fig. 2 (b).

The inlet unstart for this Case II configuration is described in detail in a previous paper,²⁴ and is only briefly discussed here. Figures 5 and 6 reveal that the boundary layer growth/separation on the bottom wall of the inlet (also the bottom wall of the tunnel) propagates upstream (see frames 13 ms (Fig. 5) and 17 ms (Fig. 6)) and generates an oblique unstart shock first appearing in front of the jet in the 13 ms panel of Fig. 5. This shock propagates upstream, and the flow unstarts shortly after the arrival of this shock at the inlet lip (Fig. 6, 17 ms). Concurrently, we also see a separated flow on the upper wall (Fig. 5, 12 ms) when the jet-induced bow shock interacts with this thin boundary layer. This upper wall disturbance also propagates upstream, preceding the unstart shock, and arrives at the tip of the splitter plate at 14 ms (Fig. 6). Trailing behind this shock is a rapidly growing boundary layer that appears to become turbulent a streamwise distance comparable to the height of the inlet channel.

D. Symmetric Wall Boundary Layer Conditions

In this section, we describe the *symmetric* inlet flow configurations, Cases III and IV (Fig. 2 (c)), which provide (ideally) identical wall boundary conditions on the top and bottom walls of the inlet. For Case III, both boundary layers are

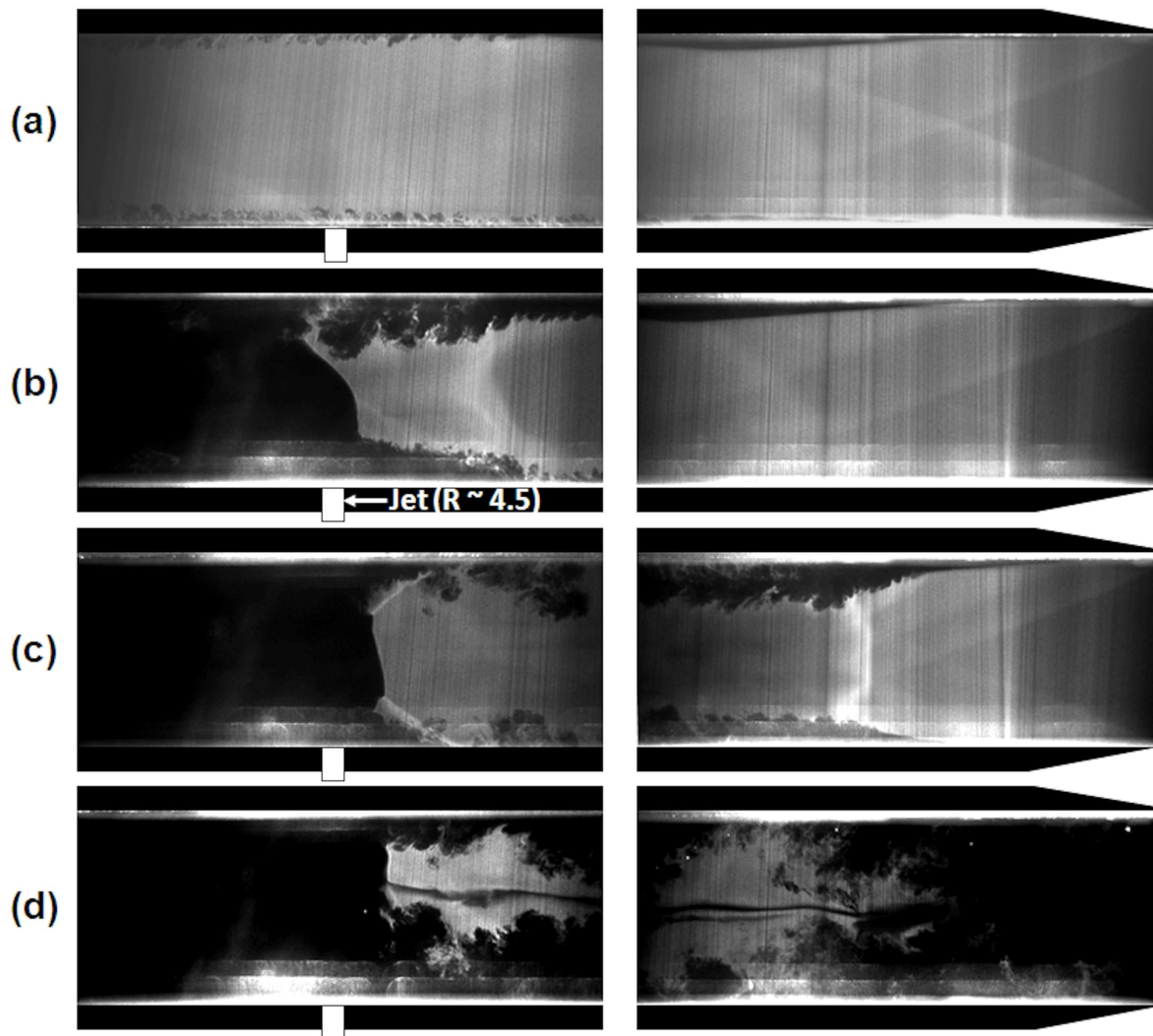


Figure 7. PLRS images with Case III configuration: (a) before the jet injection (b) the formation of a compression wave (16 – 17 ms after the jet injection), (c) a dual-shock structure (an upstream pseudo-shock and a downstream shockwave) seen in the time duration of 18 – 55 ms, and (d) breakdown of the dual-shock structure at 55 ms.

scattering from the CO₂ fog behind this wave, as this fog would be expected to evaporate in subsonic flow regions. In addition, we see from Fig. 7(c) what appears to be a normal shock (little can be said about this with the present diagnostic) or the emergence of a symmetric lambda shock downstream of this compression wave, just upstream of the jet.

So-called pseudo-shocks are often observed in internal flows²⁵⁻²⁷ and seem to accompany the growth of turbulent boundary layers when a supersonic flow decelerates to a subsonic flow in a duct. Arai et al.²⁵ observed (experimentally) that a series of compression waves intermittently pressurize and decelerates a supersonic flow in a square duct and boundary layers were found to thicken abruptly in the pseudo-shock region, in ways consistent with what we observed here in Figs. 7 (b) and 7 (c). In numerical simulations, Hataue²⁶ predicted a flow structure in a duct that consisted of a compression wave together with a downstream shock, that produced a subsonic flow. The downstream shock was strongly deformed by the interaction with the now thickened boundary layers (lambda shock). This “dual-shock” (a compression wave followed by a lambda shock) structure appears to be qualitatively similar to that shown in Fig. 7 (c).

A sudden breakdown of this dual-shock structure leading to unstart is observed at a time of 55 ms \pm 0.5 ms (see Fig. 7(d)). The breakdown occurs swiftly, within 1 ms. It is noteworthy that, in Case III, it therefore takes about 55 ms for the inlet flow to unstart – a time that is significantly longer than that of Case II (21 ms). Inlet unstart appears

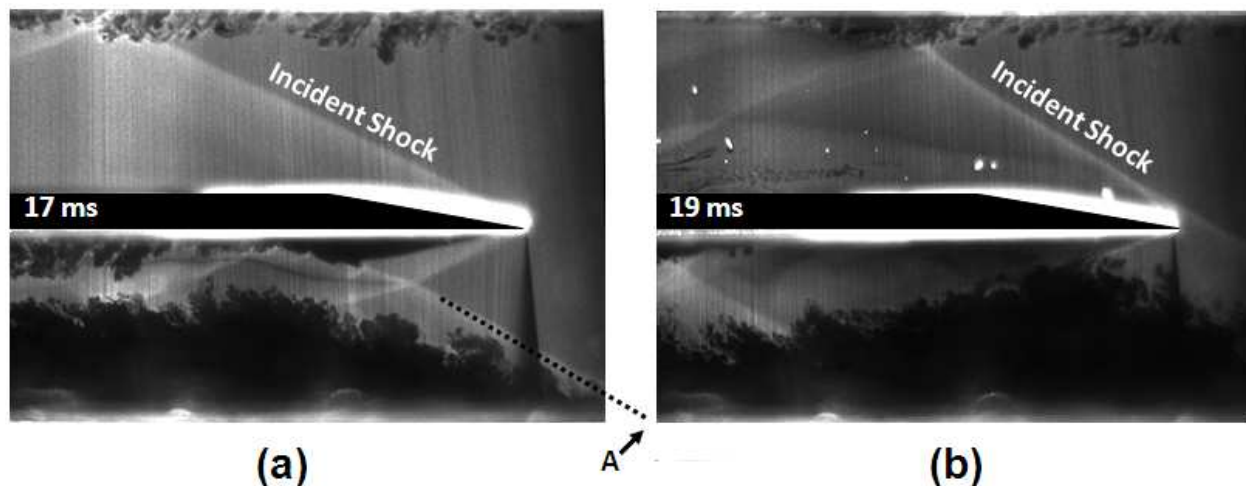


Figure 8. PLRS images revealing that the unstart shock propagates further upstream past the imaging region in Case I.

to be delayed by the isolating of inlet flow from the thick turbulent boundary layer on the tunnel walls. At this time, however, the physics related to the sudden breakdown of the flow structure is not resolved. We believe that this breakdown is caused by the relatively slow build-up in pressure at the pseudo-shock region. This mechanism will be examined in the future studies in which pressure measurements will be made along the inlet walls of the isolated flow.

From the observations made with the Case III configuration, it appears that pre-existing thick turbulent boundary

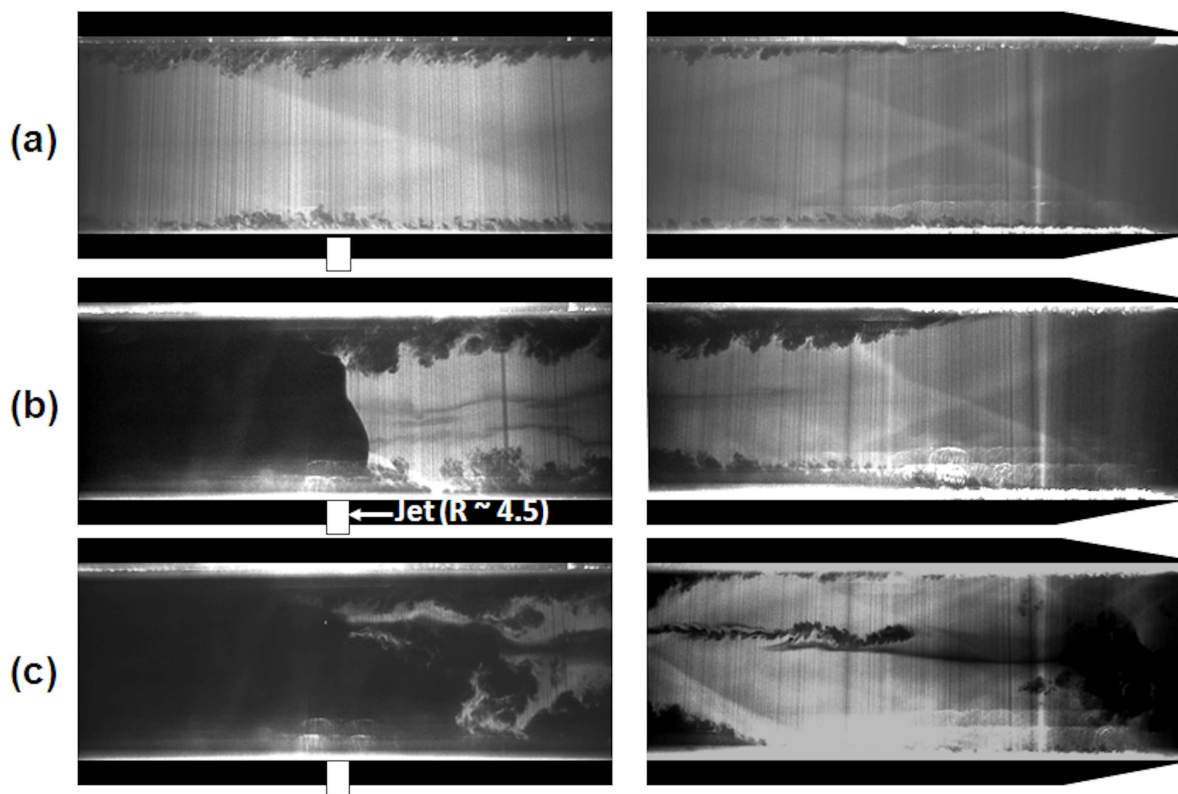


Figure 9. PLRS images with Case IV configuration: (a) before the jet injection, (b) shockwaves intersecting each other at the inlet and standing steady during 16 – 24 ms, and (c) tunnel unstart at 25 ms.

layers on the tunnel wall prompt the formation of the unstart shock seen in the Case II configuration. In Case II, this thick turbulent boundary layer is a nascent feature of the tunnel flow, growing along the tunnel wall (which serves as one wall defining the inlet) and originating in the throat region of the converging-diverging nozzle, far upstream of the inlet lip. This thick boundary layer provides a subsonic region that can possibly channel the propagation of downstream flow disturbances (e.g., pressure wave) into the region upstream of the inlet lip. For example, the unstart shock in Case II can propagate far upstream beyond the splitter plate edge, as shown in Fig. 8. The foot of the unstart shock on the bottom wall is beyond the image field in the 17 ms panel (A in Fig. 8 (a)) and continues to propagate further upstream at 19 ms (Fig. 8 (b)), where it now disturbs the flow in the upper half of the tunnel, reducing the Mach number as confirmed by the increase in the incident shock angle (Fig. 8 (b)). This makes a direct comparison of the later stages of unstart in Case III with Case II difficult, because, as shown in Fig. 8, the turbulent boundary layer on the tunnel walls (in Case II) result in an unstart shock that disrupts the upstream flow region before the complete unstart of the inlet flow – a situation not encountered in Case III.

Case IV (same geometrical configuration of Case III) also isolates the inlet from this thick turbulent boundary layer, but generates its own relatively thick turbulent wall boundary layers by the use of sandpaper near the leading edge of the splitter plates. Figure 9 (a) reveals the presence of turbulent boundary layers developing on the walls generated by sandpaper attached 5 mm downstream of the plate tips. An earlier complete inlet unstart (25 ms) compared to that seen in Case III (55 ms), is observed with this configuration. This unstart is about as fast as that seen in Case II (21 ms), although the general flow features are more similar to those seen for Case III. A compression wave (just behind the intersection of the two incident shocks), accompanying the development of thick turbulent boundary layers, propagates upstream to a quasi-stable position, anchoring there for 8 ms (16 ms – 24 ms after jet triggering), as seen in Fig. 9 (b). Then, a sudden break down of this flow structure (dual-shock) is observed at 25 ms (Fig. 9 (c)) instantly followed by complete inlet unstart. We attribute this early unstart, in comparison to that of Case III, to the initial turbulent boundary layers on the upper and lower inlet walls.

IV. Summary

A Mach 5 wind tunnel was used to generate approach flow conditions for studies of unstart in model inlet flows. In the studies described, inlet unstart is generated by the injection of an air jet. Flow dynamics following jet injection were investigated with four different inlet configurations.

Planar Laser Rayleigh Scattering imaging was used to characterize flow features, including the evolution of boundary layers and shocks. We find that unstart flow features and the overall inlet unstart process are strongly affected by the characteristics of the initial wall boundary layer prior to jet injection. In asymmetric inlet configurations, with a thick turbulent boundary layer on one wall and a thin (initially laminar) boundary layer on the other, an unstart shock emerges on the wall with an initially thick turbulent boundary layer. In Case II with the asymmetric boundary condition, complete unstart of the inlet occurs within about 21 ms. With symmetric wall configurations (i.e., cases in which wall boundary layer are similar on both sides, either turbulent or laminar), there is no oblique unstart shock. Instead, we see a relatively weak compression wave or pseudo-shock, which initially propagates upstream in advance of unstart and remains quasi-stable for some time until a catastrophic breakdown in the structure occurs and the inlet unstarts completely. The duration over which this pseudo-shock is anchored in the inlet depends on the nature of the initial boundary layer (thin laminar, or thick turbulent). With relatively thin (initially laminar) boundary layers, the pseudo-shock appears stable until 55 ms following jet injection – more than twice as long as the case in which the initial boundary layers are tripped to be turbulent (25 ms). The time for unstart in the turbulent symmetric condition is comparable to that of Case I.

Acknowledgments

This work is sponsored by the Department of Energy sponsored Predictive Science Academic Alliance Program (PSAAP) at Stanford University.

References

- ¹Emami S., Trexler C. A., Auslender A. H., and Weidner J. P., “Experimental investigation of inlet-combustor isolators for a dual-mode scramjet at a Mach number of 4,” NASA Technical Paper 3502, 1995.
- ²Wieting A. R., “Exploratory study of transient unstart phenomena in a three-dimensional fixed-geometry scramjet engine,” NASA TN D-8156, 1976.

- ³Hawkins W. R. and Marquart E. J., “Two-dimensional Generic Inlet Unstart Detection at Mach 2.5–5.0,” *6th International Aerospace Planes and Hypersonics Technologies Conference*, AIAA, Washington, DC, 1995, AIAA 95-6016.
- ⁴Rodi P. E., Emami S., and Trexler C. A., “Unsteady Pressure Behavior in a Ramjet/scramjet Inlet,” *Journal of Propulsion and Power*, Vol. 12, No. 3, 1996, pp. 486-493.
- ⁵Shimura T., Mitani T., Sakuranaka N., and Izumikawa M., “Load Oscillations Caused by Unstart of Hypersonic Wind Tunnels and Engines,” *Journal of Propulsion and Power*, Vol. 14, No. 3, 1998, pp. 348-353.
- ⁶O’Byrne S., Doolan M., Olsen S. R., and Houwing A. F. P., “Analysis of Transient Thermal Choking Processes in a Model Scramjet Engine,” *Journal of Propulsion and Power*, Vol. 16, No. 5, 2000, pp. 808-814.
- ⁷Graham R. H., *SR-71 Blackbird*, MBI Publishing Company, St. Paul, MN, 2002, pp. 27-28.
- ⁸Wagner J. L., Yuceil K. B., Valdivia A., Clemens N. T., and Dolling D. S., “PIV Measurements of the Unstart Process in a Supersonic Inlet/isolator,” *38th Fluid Dynamics Conference and Exhibit*, AIAA, Washington, DC, 2008, AIAA 2008-3849.
- ⁹Wagner J. L., Yuceil K. B., and Clemens N. T., “PIV Measurements of Unstart of an Inlet-Isolator Model in a Mach 5 Flow,” *39th Fluid Dynamics Conference and Exhibit*, AIAA, Washington, DC, 2009, AIAA 2009-4209.
- ¹⁰Andreadis D. “Scramjet Engines Enabling the Seamless Integration of Air & Space Operations,” *The Industrial Physicist*, Aug/Sept, 2004.
- ¹¹Mashio S., Kurashina K., Bamba T., Okimoto S., and Kaji S., “Unstart Phenomenon due to Thermal Choke in Scramjet Module,” *AIAA/NAL-NASDA-ISAS 10th International Space Planes and Hypersonic Systems and Technologies Conference*, AIAA, Washington, DC, 2001.
- ¹²Heiser W. H. and Pratt D. T., *Hypersonic Air Breathing Propulsion: AIAA Education Series*, AIAA, Washington, DC, 1993.
- ¹³Sato S., Izumikawa M., Tomioka S., and Mitani T., “Scramjet Engine Test at Mach 6 Flight Condition,” *33rd AIAA/ASME/SAE/ASEE Joint Propulsion Conference and Exhibit*, AIAA, Washington, DC, 1997, AIAA 97-3021.
- ¹⁴Kodera M., Tomioka S., Kanda T., Mitani T., and Kobayashi K., “Mach 6 Test of a Scramjet Engine with Boundary-layer Bleeding and Two-staged Fuel Injection,” *12th AIAA International Space Planes and Hypersonic Systems and Technologies*, AIAA, Washington, DC, 2003, AIAA 2003-7049.
- ¹⁵McDaniel K. S. and Edwards J. R., “Three-Dimensional Simulation of Thermal Choking in a Model Scramjet Combustor,” *39th Aerospace Sciences Meeting and Exhibit*, AIAA, Washington, DC, 2001, AIAA 2001-0382.
- ¹⁶Wagner J. L., Yuceil K. B., Valdivia A., Clemens N. T., and Dolling D. S., “Experimental Investigation of Unstart in an Inlet/isolator Model in Mach 5 Flow,” *AIAA Journal*, Vol. 47, No. 6, 2009, pp. 1528-1542.
- ¹⁷Curran E. T., Heiser W. H., and Pratt D. T., “Fluid Phenomena in Scramjet Combustion Systems,” *Annual Review of Fluid Mechanics*, Vol. 28, 1996, pp. 323-360.
- ¹⁸Wang X. and Le J. “Computations of Inlet/isolator for SCRAMjet Engine,” *Journal of Thermal Science*, Vol. 9, issue 4, 2000, pp. 334-338.
- ¹⁹Tam C., Eklund D., and Behdadnia R., “Influence of Downstream Boundary Conditions on Scramjet-isolator Simulations,” *26th AIAA Applied Aerodynamics Conference*, AIAA, Washington, DC, 2008, AIAA 2008-6929.
- ²⁰Valdivia A., Yuceil K. B., Wagner J. L., Clemens N. T., and Dolling D. S., “Active Control of Supersonic Inlet Unstart Using Vortex Generator Jets,” *39th Fluid Dynamics Conference and Exhibit*, AIAA, Washington, DC, 2009, AIAA 2009-4022.
- ²¹Miles R. B. and Lempert W. R., “Quantitative Flow Visualization in Unseeded Flows,” *Annual Review of Fluid Mechanics*, Vol. 29, 1997, pp. 285-326.
- ²²Wu P., Lempert W. R., and Miles R. B., “Megahertz Pulse-burst Laser and Visualization of Shock-wave/boundary-layer Interaction,” *AIAA Journal* Vol. 38, No. 4, 2000, pp. 672-679.
- ²³Poggie J., Erbland P. J., Smits A. J., and Miles R. B., “Quantitative Visualization of Compressible Turbulent Shear Flows Using Condensate-enhanced Rayleigh Scattering,” *Experiments in Fluids*, Vol. 37, 2004, pp. 438-454.
- ²⁴Do H., Im S., Mungal M.G., and Cappelli M. A., “Visualizing Supersonic Inlet Duct Unstart Using Planar Laser Rayleigh Scattering,” *Experiments in Fluids* (published online).
- ²⁵Arai T., Sugiyama H., Abe F., Takahashi T., and Onodera O., “Internal Structure of Pseudo-Shock Waves in a Square Duct,” Vol. 208, *American Institute of Physics*, College Park, MD, 1990, pp. 850 – 855.
- ²⁶Hataue I., “Computational Study of the Shock-wave/boundary-layer Interaction in a Duct,” *Fluid Dynamics Research*, Vol. 5, 1989, pp. 217-234.

²⁷Katanoda H., Matsuoka T., and Matsuo K., “Experimental Study on Shock Wave Structures in Constant-area Passage of Cold Spray Nozzle,” *Journal of Thermal Science*, Vol. 16, 2003, pp. 40-45.